Research Article Vol. 32, No. 3 / 29 Jan 2024 / Optics Express 3673
Optics EXPRESS

Multifunction integrated lithium niobate photonic chip for photon pairs generation and manipulation

TIEN-DAT PHAM,[1] CHENG-CHUNG CHIU,[1] PIN-JU TSAI,[1,2,4] AND YEN-HUNG CHEN[1,2,3,*]

[1]Department of Optics and Photonics, National Central University, Jhongli 320, Taiwan
[2]Quantum Technology Center, College of Science, National Central University, Jhongli 320, Taiwan
[3]Center for Astronautical Physics and Engineering, National Central University, Jhongli 320, Taiwan
[4]tpinju@ncu.edu.tw
[*]yhchen@dop.ncu.edu.tw

Abstract: We report on a unique photonic quantum source chip highly integrating four-stage photonic elements in a lithium niobate (LN) waveguide circuit platform, where an aperiodically poled LN (APPLN) electro-optic (EO) polarization mode converter (PMC) is sandwiched between two identical type-0 PPLN spontaneous parametric down-converters (SPDCs), followed by an EO phase controller (PC). These core nonlinear optic and EO building blocks on the chip are systematically characterized stage by stage to show its high performance as an integrated quantum source. The APPLN EO PMC, optimally constructed by a genetic algorithm, is characterized to have a broad bandwidth (>13 nm), benefiting an efficient control of broadband type-0 SPDC photon pairs featuring a short correlation time. We demonstrate an efficient conversion of the |VV› photon-pair state generated from the first PPLN SPDC stage to the |HH› state through the APPLN EO PMC stage over its operating bandwidth, a broadband or broadly tunable polarization-entangled state can thus be possibly produced via the superposition of the |VV› state generated from the other PPLN SPDC on the third stage of the chip. Such a state can be further manipulated into two of the Bell states if the relative phases between the two polarization states can be properly modulated through the EO PC on the fourth stage of the chip. Such a multifunction integrated quantum photonic source chip can be of high value to developing a compact, efficient, and high-speed quantum information processor.

1. Introduction

Quantum photonics technology has progressed rapidly and become a predominant solution for the realization of optical quantum computing, quantum communication, and quantum metrology which are believed to provide supremacy power in information processing, building (unconditionally) secure communication, and elevating sensing resolution, respectively [1–3]. Without a doubt, the preparation of a suitable quantum light source is of high relevance to optimize those photonic quantum applications, which usually involves the issues of the generation, manipulation, and encoding of the quantum information carriers such as single photons, qubits, or entangled photon pairs. The issues could be even more challenging when facing a hybrid quantum network, where the encoding degree of freedom (such as the phase or polarization [3]) of photons might be non-unitary and its setup could become complicated and massive [4,5]. The emerging photonic integrated circuits (PIC) could be a potential technology to address the faced challenges as it has become an enabling method to conduct a low-loss and high-fidelity integration of optical systems on a chip [6,7]. In terms of integrability, quantum light sources implemented via a nonlinear-optic (NLO) photon-pair generation mechanism such as the spontaneous parametric down-conversion (SPDC) or the spontaneous four-wave mixing could be a more promising choice

#509229 https://doi.org/10.1364/OE.509229
Journal © 2024 Received 12 Oct 2023; revised 7 Dec 2023; accepted 3 Jan 2024; published 19 Jan 2024

Optics EXPRESS

as they can operate in a general environment (under atmosphere, at room temperature, etc.) and can be realized in a PIC platform based on such as $LiNbO_3$ (LN) or Si-based materials [8,9], in contrast to those counterparts based on single-emitter systems like single atoms/ions or quantum dots [10].

Si photonics has been a leading technology for PIC implementation. However, several considerations may arise for the photon-pair generation in a Si-based material via the access of a relatively weak third-order ($\chi^{(3)}$) nonlinearity. First, stronger pump power is in demand to enhance the source efficiency, which might incur more difficulty in the pump filtering from the generated spectrally close pair-photons and might lead to stray radiations originating from other $\chi^{(3)}$ nonlinear (such as Raman) processes. Besides, Si photonic modulators usually operate using thermal control which limits the photon manipulation speed. These pain points can be potentially addressed with LN photonics enjoying a strong $\chi^{(2)}$ nonlinearity.

LN, renowned as "the silicon of photonics", features versatile and superior material properties including a wide spectrum transparency range, high nonlinearities, and large electro-optic (EO) effects [11], and has been a popular material platform for implementing various PIC devices and systems for a broad application range from classical to quantum photonics [12]. In photonic quantum circuits (PQC), LN-based passive and active optical components including directional couplers (and their based beam splitters), EO modulators, and (polarization) mode converters have been configured as building blocks [13] to integrate with periodically poled LN (PPLN) SPDC photon-pair sources to achieve on-chip quantum-state preparation, generation, manipulation, and verification [8,14]. However, all these components, as well as the SPDC, have finite operating bandwidths due to their respectively subjected phase-matching/dispersion conditions; for example, a type-II phase-matched PPLN SPDC has a ~3.6 nm-cm signal bandwidth in the 1.5-μm telecom band and a directional coupler, which could be the most essential building block in PQC, is usually characterized by a high sensitivity to the wavelength and fabrication errors due to its based mode interference mechanism [15]. We have proposed and demonstrated broadband directional couplers using a counterintuitive adiabatic-passage circuit scheme or a domain engineering method in LN [16,17]. The consideration of the bandwidth of each building block to be integrated on a chip is crucial to optimize the performance of the chip system.

Among the PQC building blocks, polarization mode converters/controllers (PMC) are of particular interest in creating the polarization degree of freedom greatly useful for the manipulation and encoding of quantum photons as well as the implementation of polarization entanglement [8]. However, controlling polarization in waveguides is not as trivial as in bulk optics and usually demands a more complicated or inconvenient (non-PIC compatible) scheme to implement an equivalent mechanism employed in their bulk-optic counterparts (such as a rotary linear wave plate) [18,19]. A polarization mode conversion scheme has been demonstrated in a PIC platform through a mode evolution process engineered by using a special waveguide architecture [20]. However, such a scheme works nearly passively (i.e., with poor controllability) and only for one of the polarization modes. Specifically, we have demonstrated an EO controllable PMC based on a Ti-diffused PPLN waveguide via the access of the off-diagonal Pockels tensor element r_{51} of the material [21]. Such a device is relatively simple and highly compatible with other LN photonic elements thanks to the based quasi-phase-matching (QPM) technology that benefits the integrability as any amount of the phase mismatch resultant in different integration scenarios can be possibly compensated by a specific domain structure which is engineerable in a QPM material like LN [22,23]. In this context, the ideas of the integration of a type-II PPLN SPDC photon pair source with a (or a segmented) PPLN EO PMC have been proposed to realize sources for on-chip quantum-polarization state preparation or on-chip Hong-Ou-Mandel (HOM) experiment [8,24]. However, in those schemes, both PPLN waveguide devices have a narrow/finite bandwidth (subjected to their respective QPM conditions), leading such on-chip systems to be susceptible to the operating conditions (such as temperature and wavelength) [8], not to mention the challenging

Optics EXPRESS

issue of a tight fabrication tolerance for waveguide devices [17]. The development of a broadband PMC as a building block for facilitating on-chip integration in a PQC system is thus highly desirable.

In this study, we propose and demonstrate a broadband EO PMC, realized based on a genetic algorithm [25] optimized aperiodically poled LN (APPLN), for a novel integration with a pair of type-0 PPLN SPDCs and an EO phase controller/modulator (PC) on a monolithic LN chip. This highly integrated device is capable of performing multiple functions of NLO photon-pair generation and EO photon polarization and phase controlling on a chip, which could be an important advance toward a scalable photon source scheme for building large-scale PQC. Besides the obvious advantages of the on-chip operation with a type-II PPLN SPDC as discussed above, such a broadband EO PMC can benefit the manipulation of a type-0 PPLN SPDC photon-pair source featuring also a broad phase-matching bandwidth [26] to realize a broadly tunable or a broadband polarization or time-frequency entangled state generators. The broadband control and generation of photon pairs also imply higher speeds of information processing and greater quantum information capacity.

2. Four-stage LN photon-pair source chip design and fabrication

The proposed highly integrated PQC source is implemented in a Ti-diffused LN waveguide platform, comprising three photonic elements as the core building blocks, as schematically shown in Fig. 1. The monolithic chip is configurated by a four-stage structure, where an APPLN EO PMC is sandwiched between two identical type-0 phase-matched PPLN SPDCs, followed by one EO PC situated downstream. All the stages have the same length of 1 cm. The type-0 PPLN SPDCs, on the first and third stages of the chip, have a domain grating period of 17.62 μm, designed to satisfy an *eee* QPM condition for performing a 785-nm pumped degenerate 1570-nm signal and idler parametric generation process at 106°C. The pump wavelength (785 nm) has been used in the design due to the laser availability in our lab, and an elevated operating temperature (>100°C) is desired to alleviate the possible photorefractive damage, though we didn't observe the effect during the experiment even at a lower temperature. The two PPLN SPDC stages will generate photon pairs both with the twin-photon state of $|VV\rangle$. The APPLN EO PMC stage in between the two SPDCs provides a unique mechanism to broadband control the polarization of the photon pairs generated in the first stage; one particularly interesting operation through this stage is to convert the $|VV\rangle$ state from the 1st SPDC stage to the $|HH\rangle$ state, in which a superposed quantum state, $1/\sqrt{2}(|HH\rangle - e^{i\varphi}|VV\rangle)$, can be expected at the output end of the third stage. The EO PC on the last stage, driven by a voltage source to build an electric field E_z along the LN z axis to enable the EO effect with the access of the Pockels coefficient r_{33}, is employed to work as a polarization-selective phase shifter for fast controlling/modulating the phase difference (i.e., $e^{i\varphi}$) between the two photon pairs generated by the two upstream PPLN SPDCs for an attempt to produce two of the four polarization-entangled Bell states if the output quantum state of the highly integrated four-stage LN photon-pair source is further converted through an entanglement architecture (mainly comprising a quantum eraser and a nonpolarizing beam splitter (NPBS)). The working principles of a (type-0) PPLN SPDC [27] and an EO LN phase modulator have been widely studied, we don't discuss them further here. Here in this study, we focus on a novel design of a broadband EO PMC realized in Ti:LN using the aperiodic optical superlattice (AOS) technique [28].

A conventional PPLN EO PMC has a bandwidth on the order of 2 nm·cm in the 1.5-μm band [29] which is comparable to that of a type-II PPLN SPDC but is considerably narrower than that of a type-0 one (~40 times that of a type-II one [26]). A broadband PMC is thus desired to operate with a type-0 SPDC source to extract photon pairs over a broader spectral range, which is beneficial to implement, e.g., a frequency-encoded quantum system such as a quantum key distribution based on a time-frequency correlated protocol. To broaden the

Optics EXPRESS

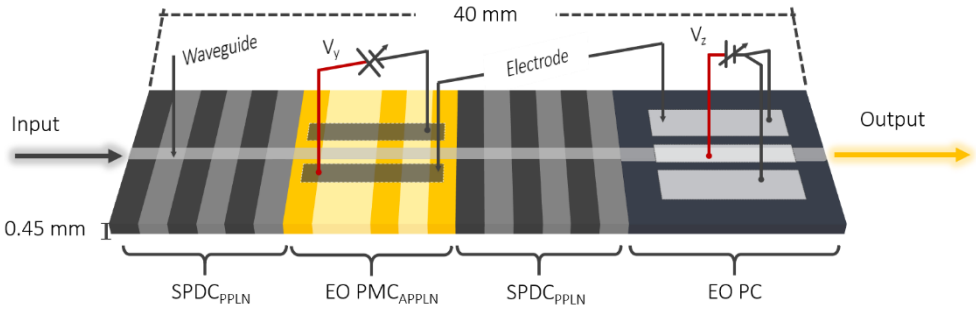

Fig. 1. Schematic of a four-stage LN photon-pair source chip monolithically integrating two identical type-0 phase-matched PPLN SPDCs, an APPLN EO PMC, and an EO phase controller.

conversion bandwidth of an EO PMC based on LN, here we develop a domain structuring model based on the genetic algorithm to construct an optimized AOS for creating multiple reciprocal vectors to simultaneously satisfy corresponding multiple (and therefore broadband) phase-matching conditions. However, the broader the phase-matching spectrum engineered in a QPM device is, the smaller the nonlinear reduction factor (; the Fourier coefficient associated with the Fourier expression of the domain structure) is, due to the resultant domain non-periodicity for accommodating more reciprocal vectors. effectively reduces the nonlinear coefficients as in a QPM wavelength converter (e.g., reduced by a factor of $2/\pi$ for a 1st order PPLN), it reduces the EO coefficients as well in a QPM PMC, leading to the increase of the required applied electric field (or equivalently, half-wave voltage V_π). It is thus our pursuit of the genetic algorithm to construct an EO PMC having an as broad as possible bandwidth (at least broader than a targeted bandwidth, see below) under a reasonably low operating voltage V_π. In the algorithm, we first determine the number of domain segments, N, to form the $L_{PMC} = 1$-cm long APPLN EO PMC, which corresponds to the number of genes encoded in each chromosome that plays as an individual of the population initiating the genetic evolution. Figure 2 schematically shows the domain configuration of an AOS in LN (i.e., an APPLN), built by N domain blocks of a unit thickness of Δx with respective domain polarities determined by the genetic algorithm. According to the QPM theory, the coherence length $l_{c,PMC}$ of the EO PMC process in Ti:LN [21] is ~11.2 μm, estimated from the wave-vector mismatch $\Delta k_{PMC} = k_{1,V} - k_{1,H}$ between the photons of V(TM) and H(TE) polarization modes in a band around 1570 nm generated from the PPLN SPDC on the 1st stage at 106°C. Accordingly, we set $N = 892$ ($\sim L_{PMC}/l_{c,PMC}$) for the algorithm to find an optimized sequence of N binary (e.g., + 1 and -1, representing the positive and negative domain polarities, respectively) data (corresponding to a gene string containing 892 codes ia chromosome) that contain the information of the domain structure formed in the APPLN. This is equivalent to finding a domain-polarity sequence (a gene string) through the genetic evolution process that can provide all the reciprocal vectors ($K_p 2\pi/\Lambda_p = \pi/l_{c,PMC,p}$. for the p-th EO PMC process, where Λ is the periodicity or the inverse of the spatial frequency) required to tailor a phase-matching spectrum for an EO PMC to achieve the targeted (broad) operating bandwidth with respect to 1570 nm. The use of a 1-cm long device is a trade-off among a sufficient number (N) of variables for diversifying the gene encoding process to expedite the algorithm to reach a (globally) optimal solution, a broader bandwidth and better compactness for a shorter device length, and a lower working voltage (V_π) for a longer device length.

In the algorithm, the initial domain-polarity distribution (i.e., a sequence of N binary code) of each created domain structure is randomly generated by the computer, which accomplishes the initial gene-string coding for each individual (chromosome). To ensure a comprehensive genetic evolution, all the initially created individuals in the original population are further divided into

Optics EXPRESS

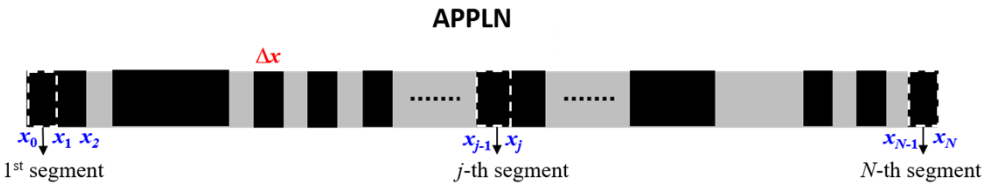

Fig. 2. Schematic illustration of APPLN domain construction using the genetic algorithm.

6 subpopulations with each comprising 1000 individuals for the subsequent operations. In the algorithm, we employ operators including selection, crossover, mutation, and migration [30] in the evolution process to evolve the population into a generation of offspring with an optimum gene string (corresponding to the APPLN domain structure), guided by a fitness/objective function (OF), given by

$$OF = \left\{\sum_{p=1}^{M} w(\lambda_p)|\eta_0(\lambda_p) - \eta_c(\lambda_p)|\right\} + \beta\{\ \max[\eta_c(\lambda_1), \ldots, \eta_c(\lambda_M)] - min[\eta_c(\lambda_1), \ldots, \eta_c(\lambda_M)]\}, \tag{1}$$

where M is the number of the multiple EO PMC processes set for tailoring a targeted broadband conversion spectrum in the APPLN, $\eta_0(\lambda_p)$ and $\eta_c(\lambda_p)$ are the target and calculated conversion efficiencies of the p-th EO PMC process at wavelength λ_p, respectively, $w(\lambda_p)$ is the weighting factor on the efficiency for the p-th process, β is the weighting factor on the equalization of the peak conversion efficiencies of the M EO PMC processes, and the operators max[. . .] and min[. . .] select the maximum and minimum values from the quantities enclosed in the square brackets. η_c can be calculated using the coupled-mode equations governing the interaction of the two cross-polarized eigenmodes [31]:

$$\begin{aligned}\frac{dE_{V,p}(x)}{dx} &= -i\frac{2}{\lambda_p\sqrt{n_{V,p}n_{H,p}}}s(x)[\kappa_{PMC,p}E_{H,p}(x)e^{i\Delta k_{PMC,p}x}],\\ \frac{dE_{H,p}(x)}{dx} &= -i\frac{2\pi}{\lambda_p\sqrt{n_{V,p}n_{H,p}}}s(x)[\kappa^*_{PMC,p}E_{V,p}(x)e^{-i\Delta k_{PMC,p}x}],\end{aligned} \tag{2}$$

where i is the imaginary unit, the subscript p denotes quantities associated to the modes with a wavelength at λ_p, $E(x)$ is the mode amplitude, n is the effective refractive index, $s(x)= \pm 1$ is a sign function denoting the $\pm z$ crystal polarity of the domain segment at position x (see Fig. 2), and $\kappa_{PMC} = -(1/2)n^2_{p,V}n^2_{p,H}r_{51}E_y$ is the coupling coefficient of the conversion process, where r_{51} is the relevant Pockels coefficient and E_y is an external electric field applied along the crystallographic y axis of the APPLN. By iteratively solving Eq. (2) segment by segment (located at x_j for $j = 0, 2, \ldots, N\text{-}1$; see Fig. 2) through the APPLN domains for a given input field of $E_{V,p}(x_0 = 0)$, we can calculate the conversion efficiency of the EO PMC as $\eta_c(\lambda_p) = |E_{H,p}(x_N)|^2/|E_{V,p}(x_0)|^2$.

In the algorithm, we pursue an APPLN EO PMC that has a bandwidth at least broader than that of a component with the narrowest bandwidth in the experimental setup (which is a 12-nm bandpass filter, see below) for characterizing the Four-stage LN photon-pair source chip under an as low as possible operating voltage V_π. Figure 3(a) shows the calculated conversion spectrum of the APPLN EO PMC designed by the genetic algorithm when applied with a V_π=25 V. The conversion spectrum of a PPLN EO PMC (V_π= 8.8 V) is also plotted for comparison. The results show the bandwidth of the APPLN EO PMC is ~13 nm as targeted and is >5-fold broader than that of a PPLN counterpart with a V_π increased by less than 3 times, showing the powerfulness of the developed genetic algorithm. This optimized result is obtained by setting the

Optics EXPRESS

selection, crossover, mutation, and migration rates for the genetic operations in the algorithm to be 20%, 80%, 0.07%, and 0.1%, respectively, and by setting the OF in Eq. (1) with $M = 10$ (with $\lambda_p = 1567.5, 1568, \ldots, 1572, 1572.5$ nm at a step of 0.5 nm), $\eta_0(\lambda_p) = 1$, $w(\lambda_p) = 1$, β=0.4, and V_π=25 V. Since the conversion bandwidth of each set spectral component λ_p is ~2.5 nm, a wavelength step of 0.5 nm is already fine enough for the algorithm to find an APPLN structure capable of making up a ~7-nm conversion bandwidth of ~100% efficiency and a ~13-nm full width at half maximum (FWHM) bandwidth (see Fig. 3(a)). All the parameters used in our simulation are adjusted and optimized by monitoring the balance between iteration number and convergence rate through computer code control. The parameter tuning process is similar to that reported in [32,33]. Figure 3(b) shows the Fourier spectrum of the APPLN domain structure, revealing a prominent spectral peak emerging at spatial frequencies ranging from 0.0444 to 0.0449 μm^{-1} (corresponding to QPM grating periods Λ ranging from 22.27 to 22.52 μm), which is expected to simultaneously satisfy a wide range of QPM conditions that can make up a conversion spectrum with a bandwidth >15 nm around 1570 nm for the APPLN EO PMC. The inset shows the domain binary (positive and negative domain polarities) structure of some sections of the calculated APPLN.

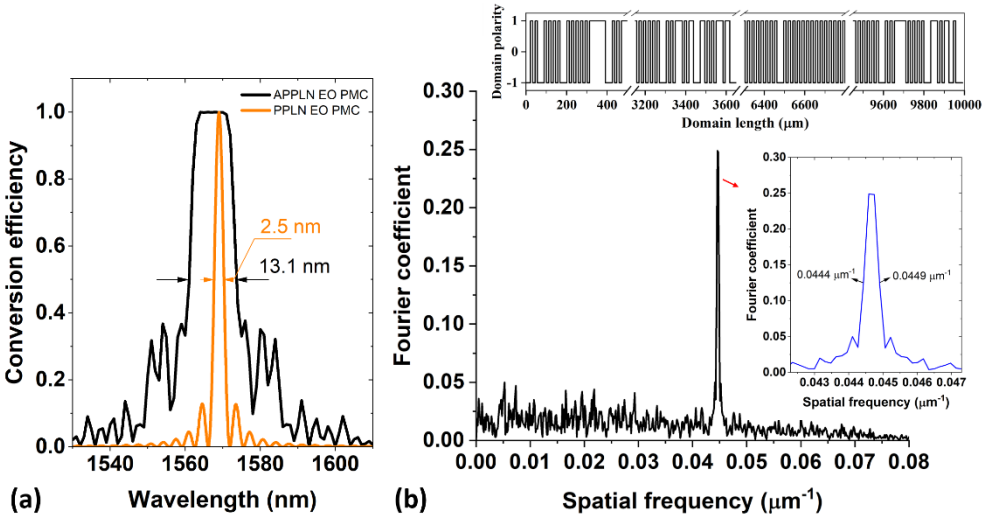

Fig. 3. (a) Calculated conversion spectra of the APPLN EO PMC designed by the genetic algorithm (black curve) and an PPLN EO PMC (orange curve). Both devices have a length of 1 cm. (b) Fourier spectrum of the APPLN domain structure. The inset at the top shows the domain-polarity structure of some sections of the calculated APPLN.

To characterize and demonstrate the proposed novel four-stage LN photon-pair source, we fabricated such a highly integrated device comprising the two type-0 PPLN SPDC, the APPLN EO PMC, and the EO PC on a 40-mm-long (along the crystallographic x axis) z-cut single LN chip, as schematically shown in Fig. 1. The fabrication steps mainly include the waveguide formation, domain poling, and electrode application. The titanium thermal indiffusion method [34] has been employed in this work to implement low-loss waveguides in LN for supporting the guiding of both the V(TM) and H(TE) polarization modes. First, a group of Ti strips with a width of ~7 μm and a thickness of 100 nm were applied on the -z surface and along the entire length (x direction) of the LN chip. The Ti:LN waveguides were then formed by heating the sample in a 3-zone furnace at 1035°C for 12 hours. The waveguides were characterized to be able to guide single fundamental modes over the telecom S-C-L bands (~1450-1650 nm) and have propagation losses of <0.3 dB/cm for both polarization modes at around 1570 nm. The QPM

Optics EXPRESS

domain architecture on the first three stages of the chip device, i.e., a 17.62-μm-period PPLN, an APPLN, and a 17.62-μm-period PPLN, was then fabricated by using the standard electric-field poling technique after the removal of the domain-inverted layer formed on the $+z$ face of the LN during the thermal indiffusion process [35]. Optical grade polishing was next applied on the two end faces of the chip. Finally, the fabrication of the chip device was done by coating strip Ni/Au (of thicknesses 50 nm/150 nm) electrodes in appropriate architectures on the APPLN EO PMC and the EO PC stages to allow the voltage applications to establish the driving fields E_y and E_z, respectively. A 100-nm-thick SiO_2 film was properly applied between the waveguides and the metal electrodes as a buffer layer. Figure 4 shows the microscopic images of portions of the fabricated PPLN (SPDC) and APPLN (PMC) domain structures revealed by HF etching on the $+z$ surface of the chip and the electrode configurations on the -z surface applied to the EO PMC and the EO PC, respectively.

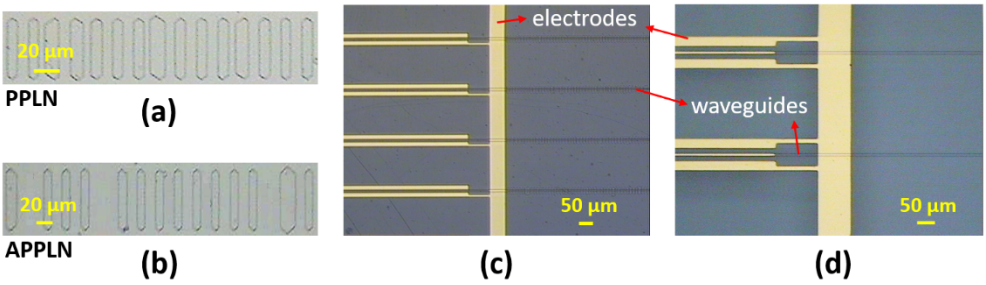

Fig. 4. Microscopic images of portions of the fabricated (a) PPLN SPDC and (b) APPLN PMC domain structures and the electrode configurations applied to the (c) PMC and the (d) PC stages.

3. Four-stage LN photon-pair source chip characterization

To validate the performance of the prepared four-stage LN photon-pair source, we systematically conducted a series of tests to characterize the performance of this chip stage by stage. These tests included experiments for evaluating the relationship between the bandwidth, conversion efficiency, and operating voltage of the APPLN EO PMC, the generation and manipulation of photon pairs from the PPLN SPDC stages, and the phase controlling in the EO modulator stage.

3.1. Pump and testing light sources

In order to effectively segment the performance testing of each stage of the chip, we prepared two laser sources for experimental purposes, as shown in Fig. 5(a). An external cavity laser (ECL), operating in the range of 1530 nm to 1600 nm, was used for simulating operations in the communication band, serving as a testing light source before conducting any manipulation and testing of the quantum light source. On the other hand, a volume-holographic-grating (VHG) laser, operating at 785 nm, was used to drive the photon pair generations in the SPDC stages. Depending on testing purposes, the two lasers will be coupled into the waveguide input end through the fiber-optic guidance, respectively. For the output, an object lens captures the light and aligns it into a collimated beam for further measurements.

3.2. Verification of EO PMC stage

Before proceeding with the measurement of the quantum properties of the chip, our initial focus is on verifying the controlling function of the chip by using the ECL laser. In the case of the APPLN EO PMC, the objective is to convert the polarization state (which is $|VV\rangle$) of the photon pairs

Optics EXPRESS

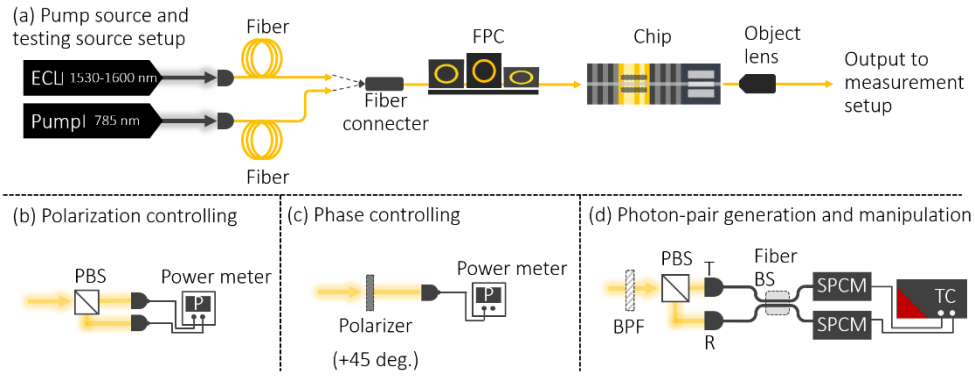

Fig. 5. Experimental setup for the chip characterization. (a) Pump laser source and testing light source setup. Both lasers are coupled into a fiber and linked to a fiber polarization controller (FPC) for controlling the polarization. The measurement setups for characterizing the chip's performance are shown in the lower row of the figure. (b) Setup of verification of polarization controlling. The output field is separated by a polarizing beam splitter (PBS) for analyzing the polarization state of light. (c) Experimental setup of verification of phase controlling. (d) Experimental setup of verification of photon-pair generation and manipulation. SPCM: Single photon counting module; TC: Time Controller; BFP: Bandpass filter; Fiber BS: Fiber beam splitter.

generated from the PPLN SPDC on the first stage to a desired state (which is $|HH\rangle$). However, for the photon pairs to be efficiently controlled by the EO PMC, several conditions must be satisfied. Firstly, at a given operating temperature, the wavelength of the (degenerate) photon pairs generated by the SPDC needs to match the spectrum of EO PMC. In the general PPLN structure, the conversion spectrum of the EO PMC is theoretically a sinc square function, with a relatively narrow bandwidth (~2.5 nm·cm at 1570 nm, see Fig. 3(a)). This implies that the operating wavelength of type-0 SPDC photon pairs is required to be nearly degenerate. Though the APPLN EO PMC, optimized using a genetic algorithm, has a 5-fold broader bandwidth in contrast to its PPLN counterpart (see Fig. 3(a)) and can alleviate the issue, non-degenerate photon pairs may still prevent such an EO PMC from converting the photon pairs more efficiently. Therefore, to efficiently control the photon pairs, the chip needs to maintain degenerate SPDC while ensuring that the conversion spectrum of the EO PMC covers the center wavelength of the SPDC at a given temperature. Additionally, the designed bandwidth of the APPLN EO PMC conversion spectrum also needs to be experimentally verified.

To experimentally determine the operation temperature of the degenerate PPLN SPDC photon pairs generated on the first stage under the driving of a 785 nm pump laser, second harmonic generation (SHG) serves as a reverse processing method for acquiring the information. In this SHG experiment, we tested a separate PPLN SPDC chip (1-cm long) produced using the same fabrication conditions reported above, in order to avoid possible interference between SHG signals generated from two-segmented identical PPLNs [36] if we conduct the experiment directly from the 4-stage chip. The specification of this stand-alone PPLN chip is the same as those constructed in the 4-stage chip. The testing light source (the ECL laser) is first set to operate at a wavelength of 1570 nm and amplified to ~50 mW through an erbium-doped optical fiber amplifier (EDFA). Then, the polarization of the light source is adjusted to V-polarization before it is coupled to the chip to generate the SHG signal using the type-0 phase-matching scheme. By varying the chip temperature and observing the conversion efficiency of SHG, we found the phase-matching temperature for 1570 nm to be at ~106°C as designed. Figure 6 shows the measured normalized SHG spectrum (orange dots) of the stand-alone PPLN chip by tuning the

Optics EXPRESS

ECL laser around 1570 nm under a fixed chip temperature at 106°C. The result implies the PPLN SPDC will generate degenerate photon pairs at 1570 nm at 106°C when pumped by a 785 nm laser, as also evidenced by the theoretical fit (orange line).

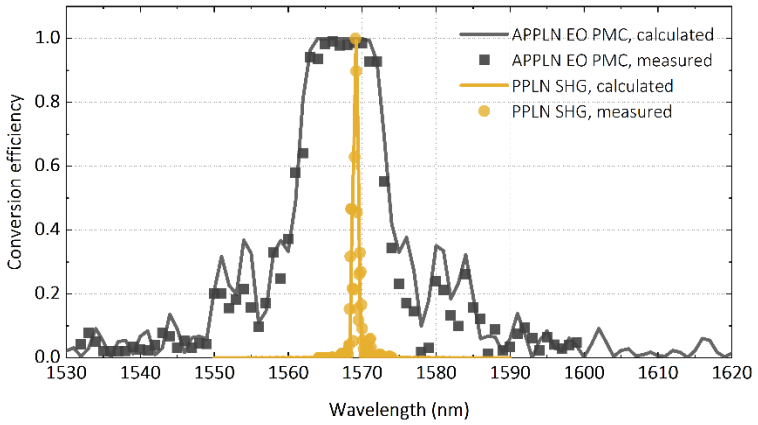

Fig. 6. Measured and calculated conversion spectra of the APPLN EO PMC (gray squares and solid line) and the SHG of a separate PPLN SPDC chip (orange dots and solid line) at 106°C. A normalized SHG efficiency is used. It exhibits excellent agreement between the experimental results and the theoretical prediction for both data.

We next characterize the performance of the APPLN EO PMC on the fabricated 4-stage photon-pair source chip by establishing a polarization control test setup as shown in Fig. 5(b). According to the type-0 phase matching condition of the first-stage SPDC, the generated photon pairs will carry the quantum state of $|VV\rangle$. To emulate the process of photon pairs passing through the EO PMC classically, we again control the testing light source to be at V-polarization before sending it into the chip. At the output end of the chip, a PBS is used to observe the polarization changes of the light controlled by the EO PMC and estimate the conversion efficiency. In order to avoid the unwanted SHG process generated by the testing light source in the PPLN SPDC stages, we removed the EDFA and kept the laser power at a low level (<1 mW before entering the chip) to have negligible nonlinear effects. The $V_{\pi,\,\mathrm{PMC}}$ is first characterized to be ~55 V by monitoring the variation of the conversion efficiency of the APPLN EO PMC as a function of the applied voltage for a wavelength at 1570 nm at 106°C. The conversion efficiency (η_{PMC}) of the device is obtained by comparing the ratio of the power in H-polarization after the PBS under the voltage control to that in the initial V-polarization state without the function of EO PMC. A higher V_π is measured than that designed (25 V) implying an overlap efficiency (related to the spatial overlap among the two polarization-mode fields and the external field (E_y) [21]) of our device to be ~0.45. The overlap efficiency can be further enhanced by using a more optimized electrode scheme [37] or nanometric ridge waveguides formed in such as thin-film LN on insulator (LNOI) [38]. Figure 6 shows the measured conversion spectrum (gray squares) of the APPLN EO PMC operating at 55 V at 106°C, which is in excellent agreement with the prediction (gray line; as in Fig. 3(a)). Besides having a full-width at half-maximum (-3-dB bandwidth) of >13 nm, the device also exhibits a -20-dB (99%) bandwidth of ~7 nm in the 1570-nm band. Besides the commendable agreement between the calculation and experimental results as shown in Fig. 6, it could be noticed that the polarization conversion spectrum of the APPLN device displays a notably distinct distribution from the typical sinc-square function of a PPLN device, reflecting the success of the genetic algorithm developed in this study. Furthermore, in comparison to the peak position of the SHG signal, it clearly implies that the designed APPLN EO PMC will efficiently control the polarization of the degenerate PPLN SPDC photon pairs generated from

Optics EXPRESS

the first stage of the chip. Besides, both the spectra of the APPLN EO PMC and PPLN SHG are temperature tunable with a tuning rate of ~-1 nm/°C and ~+0.2 nm/°C, respectively. The spectra of the two devices can overlap in the temperature range of 102°C to 107°C, we fixed the operating temperature of the chip at 106°C under which the PPLN SPDC sections operate at the wavelength-degenerate (~1570 nm) condition.

3.3. Verification of photon pairs generation and manipulation

With the demonstration of a broadband polarization controller based on the genetic-algorithm optimized APPLN EO PMC arranged on the second stage of the chip, we next shift to test the generation and control of photon pairs together with the two type-0 PPLN SPDCs on the first and third stages, the setup is illustrated in Fig. 5(d). To generate photon pairs, the 785-nm VHG pump laser is controlled at V-polarization to meet the type-0 phase-matching condition for producing photon pairs at $|VV>$ states through the PPLN SPDC sections. At the output of the chip, a 1570-nm bandpass filter (BPF) with a linewidth of ~12 nm is inserted to filter out the pump laser while allowing the transmission of the SPDC photon pairs, thus avoiding potential interference from much brighter pump photons and other background stray lights on the measurement results acquired based on a very sensitive single photon counting technique.

In order to demonstrate the manipulation of photon pairs from the first-stage SPDC with the APPLN EO PMC, a polarizing beam splitter (PBS) is installed after the BPF. The two output ends of transmission and reflection of PBS represent the separation of the quantum states of $|HH>$ and $|VV>$, respectively. Thus, the setup can analyze the operation of the EO PMC on the first-stage SPDC which produces only the $|VV>$-state photon pairs. To detect and analyze the photon pairs, the two outputs of the PBS are linked into the two arms of a 50/50 fiber beam splitter (FBS), respectively, and the two output ends of the FBS are connected to two single photon detectors (ID230, IDQ, with a quantum efficiency of ~25%) for single photons measurement. The reason for employing FBS is that type-0 photon pairs have the same polarization, and the chip operates under wavelength-degenerate conditions, which makes the two photons indistinguishable. Therefore, FBS can conditionally separate the two-photon events into the two output ends of the FBS. Furthermore, the signals from the two single-photon detectors are connected to a timing controller (ID900, IDQ) for conducting the coincidence counting measurement to analyze the photon temporal correlation and thereby capture the photon pair signals from a SPDC.

In the verification of photon pair generation, the pump is set at <~0.1 mW to minimize the possibility of the generation of multiphoton-pair events. The chip operates under wavelength-degenerate conditions at 106°C to ensure an efficient control with the EO PMC. We first test the characteristics of the photon pair generation from the SPDCs. To do this, the EO PMC is initially disabled (i.e., without the application of a voltage), and the PBS transmission and reflection arms are separately blocked to measure the quantum state events of $|VV>$ prepared by the unmanipulated type-0 SPDCs and estimate the background noise level in $|HH>$ channel, respectively. Under conditions of 3 minutes of accumulated time and 13 ps of time resolution, we obtained the coincidence count results as shown in Fig. 7(a). In Fig. 7(a), the orange squares and dark blue circles represent the coincidence count results of $|VV>$ and $|HH>$ events, respectively. It can be clearly observed that the temporal statistics of the $|VV>$ quantum state prepared by the first and third stages together exhibit a relatively narrow distribution, with a coincidences-to-accidentals ratio (CAR) of up to 3000. Actually, the coincidence counts have a finite time width of around 150 ps, which is primarily contributed by the finite timing jitter of the single photon detectors. The result also reveals that the photon pair features a short correlation time, implying a broad bandwidth. On the other hand, without the effect of the EO PMC, no $|HH>$ events are detected, indicating that the initial state of the chip has relatively low background noise. Based on the measured data, we can estimate that the photon pair detection rate of the developed photon pair source is approximately 504.2 pairs-Hz/mW. Based on this

Optics EXPRESS

measured photon pair detection rate, we estimate the original photon pair generation rate of our PPLN SPDC source to be 1.26×10^8 Hz/mW according the losses analyzed from the chip to the detection system including the measured chip insertion loss, ~-5.8 dB, quantum efficiency of the single-photon detectors, 25%, the transmittance of the bandpass filters with a linewidth of 12-nm (where a broad spectral range of the type-0 SPDC photons is rejected), 7%, and the optical losses due to the finite transmittance or coupling efficiency of other optical elements in the setup, characterized to be ~-3.3 dB. It is important to note that, since the measurement of coincidence counting involves two photons of signal and idler, the overall external efficiency is the square of the efficiencies analyzed above. This deduced photon pair generation rate has been about one order of magnitude lower than the ideal theoretical value of $\sim 4 \times 10^9$ Hz/mW calculated for our PPLN SPDC using the theory developed in [39]. This implies a more careful loss analysis of our experimental system is required.

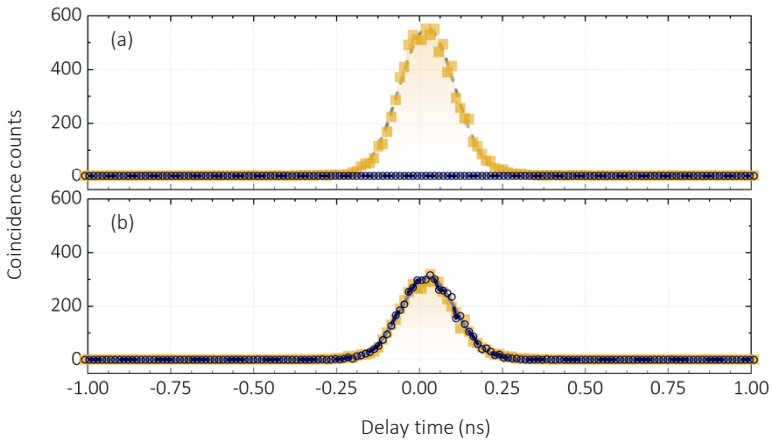

Fig. 7. The coincidence counting measurement in the case of (a) EO PMC disabled and (b) EO PMC enabled. The orange squares denote the events of quantum state |VV>, while the dark blue circles represent the events of quantum state |HH > . In (b), the quantum state |HH > is efficiently converted from the first-stage SPDC producing only the |VV > state by enabling the EO PMC stage. The time bin is set at 13 ps and the accumulation time is 3 mins for both cases.

Since a type-0 degenerate SPDC source features a broad bandwidth (estimated to be >~100 nm [40] for our device), which will still be much greater than the 13-nm conversion bandwidth of the APPLN EO PMC (though it is already several-fold broader than a conventional PMC). This may potentially render the type-0 SPDC photon pairs unable to be perfectly converted, and may also require a different optimal applied voltage than that characterized above by the ECL source. Nevertheless, thanks to the filtering of the BPF with a central wavelength of 1570 nm and a linewidth of 12 nm, we expect that the majority of SPDC photon pairs after the noise-rejection BPF will be covered by the effective spectrum (see Fig. 6) of the APPLN EO PMC, achieving high-efficiency conversion.

To confirm the optimal operating voltage of the APPLN EO PMC for the manipulation of the first-stage SPDC photon pairs, the |VV > channel of the PBS in Fig. 5(d) is blocked to observe the converted photon counting rate of |HH > . Figure 8 shows the measured counting rates of the pure |HH > events as a function of the operating voltage of the EO PMC at 106°C. It can be found that an optimal counting rate reaches at around 55 V, agreeing well with that characterized by the classical measure.

We then employ the same measurement method and photon statistical conditions as those used in the case of a disabled EO PMC, and measure the coincidence-count results of |VV > and

Optics EXPRESS

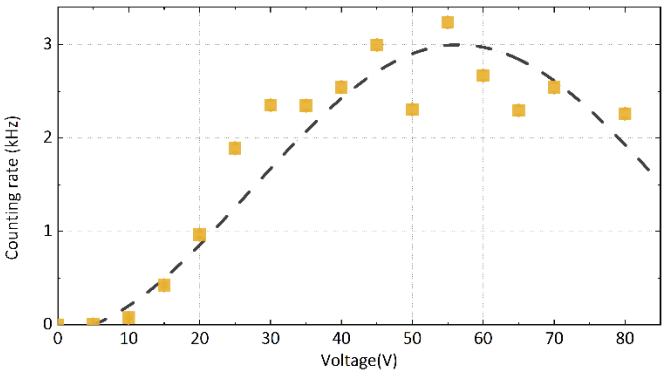

Fig. 8. Measured counting rates (orange squares) of the pure |HH > events as a function of the operating voltage of the EO PMC at 106°C. The black dashed line is a sine square function fitting, which gives $V_{\pi,\mathrm{PMC}} = 55$ V.

|HH > events separately when the EO PMC is enabled by applying a voltage of $V_{\pi,\mathrm{PMC}} = 55$ V, as shown in Fig. 7(b). From Fig. 7(b), it can be observed that the |HH > photon pairs converted from the first-stage SPDC can now be detected, while the third-stage SPDC maintains its original |VV > quantum state. The ratio of the counting rates between the |HH > and |VV > states is well-maintained at around 49.5/50.4. In comparison to Fig. 7(a), the counting rate of |HH > is approximately 50% of that when EOPMC is disabled. This also manifests that the EO PMC has a highly efficient control over the photon pairs generated from the first-stage PPLN SPDC, effectively transforming the polarization quantum state of the photon pairs over a bandwidth of ~12 nm.

3.4. *Verification of PC stage*

According to the design of the 4-stage chip and the experimental verification made above, the quantum state |VV⟩ produced by the first-stage SPDC can be converted by the second-stage EO PMC to the quantum state |HH⟩. Meanwhile, on the third stage, the SPDC will still generate photon pairs in the state |VV⟩ without an effect from the prior EO PMC stage. Since the two stages of SPDC are driven by a single pump field, the generated quantum states of $|HH\rangle$ (from the 1st stage) and $|VV\rangle$ (3rd stage) have a stable phase coherence and further create a pure Bell state $|\psi\rangle = (|HH\rangle - e^{i\varphi}|VV\rangle)/\sqrt{2}$, where φ represents the phase difference between the photon pairs generated from the two SPDCs on the first and third stages of the chip, respectively. To control this entangled state into the Bell states $|\Phi^+\rangle$ or $|\Phi^-\rangle$ in order to address wider potential applications, the relative phases φ between |HH⟩ and |VV⟩ must be modulatable beyond π under reasonable operating conditions. The EO phase controlling (PC) device on the fourth stage of the chip provides a solution to modulate this phase difference. The PC utilizes the application of a potential difference in the crystal z-direction, inducing the EO phase retardation between the H- and V-polarized photons, tunable simply by the control of the applied voltage.

To verify the phase control of the two polarization states on the chip as described above, we have established the setup depicted in Fig. 5(c). For the PC verification, the testing light source is again the ECL but with its polarization controlled to be at +45° with respect to the crystal z axis to excite and simulate the quantum state $1/\sqrt{2}(|H\rangle + |V\rangle)$ in the waveguide chip (at this point, the EO PMC is disabled). Then, by applying an increased voltage on the PC stage, it modulates the relative phase between |H⟩ and |V⟩, further altering the polarization state of the testing light. A + 45° polarizer is placed at the output end of the chip as a polarization analyzer. Figure 9 shows the power transmission measured after the polarization analyzer as

Optics EXPRESS

a function of the applied PC voltage. According to the measurement results, we can estimate the relationship between the applied voltage, V, and the phase difference between the states $|H\rangle$ and $|V\rangle$ as $\Delta\phi = \frac{\pi}{V_{\pi,PC}}(V - V_0)$, where $V_0 \sim 6.4V$ is the offset voltage and $V_{\pi,PC}$~25 V. When applied with a voltage of approximately 31.4 V, the PC stage manipulates the test light state of $1/\sqrt{2}(|H\rangle + |V\rangle)$ into the state of $1/\sqrt{2}(|H\rangle - |V\rangle)$. This implies that the developed PC can achieve relative phase control between |H⟩ and |V⟩ to the level of π under reasonable conditions ($V_{\pi,PC} = 25$ V). In addition, we can expect that the polarization state of each point can be expressed as $\frac{1}{\sqrt{2}}\left(|H\rangle + e^{i\frac{\pi}{V_{\pi,PC}}(V-V_0)}|V\rangle\right)$, which can arrive at all equatorial qubits on the Bloch sphere. It is found that the troughs of the voltage tuning curve in Fig. 9 can't reach zero, which can be attributed to the nonuniform electric field established in the electrode configuration built on the PC stage (see Fig. 4(d)), resulting in incomplete control of the phase difference between horizontal and vertical polarization components. Based on the results in Fig. 9, meanwhile, it can be estimated that the visibility for phase manipulation is about 87%, demonstrating excellent control performance of the PC stage.

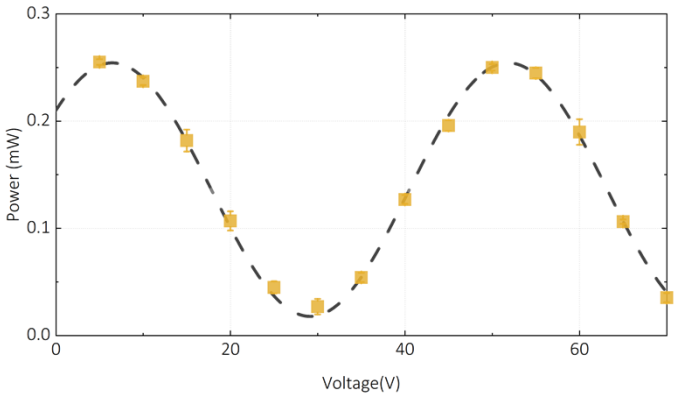

Fig. 9. Power transmission measured after the polarization analyzer as a function of the applied PC voltage (refer to the setup depicted in Fig. 5(c)). The orange squares represent the experimental data, and the black dashed line is a sine square function fitting, which gives $V_{\pi,PC}$ =25 V.

The 4-stage PQC photon-pair source chip demonstrated in this work can be viably implemented in nanometric waveguide circuits using the advanced LNOI technology [41,42] to further increase its integrability thanks to the featured miniaturized footprint [43] and ultra-low operating voltages [38].

We believe that the powerful chip developed in this study can be of great interest to many applications including broadband optical quantum information processing [44], quantum sensing [45,46], and quantum computing and communication [47–49].

4. Conclusion

We have demonstrated a novel highly integrated 4-stage quantum light source based on a LN PIC chip. The chip is capable of simultaneously achieving broadband photon pair generation, EO polarization control of the photon-pair quantum states, and EO phase control of the entangled photon pairs. According to the results from the stage-by-stage validation of this chip, the polarization control stage based on a genetic-algorithm optimized APPLN EO PMC can provide a relatively broad -3-dB bandwidth of >13 nm and a -20-dB bandwidth of ~7 nm in the 1570-nm band at a reasonable operating voltage ($V_{\pi,\mathrm{PMC}} = 55$ V). The unique, flat-distribution EO PMC spectrum enables this device to more effectively control a broadband SPDC source integrated on

Optics EXPRESS

the same chip, further offers an excellent solution for broadband quantum information processing. Furthermore, the two-stage SPDC design gives this chip the potential to generate Bell states on a single chip, while the phase control stage can provide manipulation for these Bell states in a $V_{\pi,\mathrm{PC}} = 25$ V. The development of this chip can also find applications in quantum key distribution protocols and optical quantum computing, providing a versatile and compact source and control solution for applications in optical quantum technologies.

Funding. National Science and Technology Council (111-2627-M-008-001, 111-2923-E-008-001, 111-2923-M-032-002-MY5, 112-2119-M-008-007).

Acknowledgments. The authors thank the Taiwan Semiconductor Research Institute (TSRI), Taiwan, the Nano Facility Center at National Yang Ming Chiao Tung University, Taiwan, and the Instrumentation Center at National Tsing Hua University, Taiwan for the support of the microfabrication facility.

Disclosures. The authors declare no conflicts of interest.

Data availability. Data underlying the results presented in this paper are not publicly available at this time but may be obtained from the authors upon reasonable request.

References

1. OIDA, "OIDA Quantum Photonics Roadmap: Every Photon Counts," *Optica Industry Report*, 3 (2020).
2. Y. H. Chen, C. H. Cho, W. Yuan, *et al.*, "Photonic Quantum Computers Enlighten the World: A review of their development, types, and applications," IEEE Nanotechnol. Mag. **16**(4), 4–9 (2022).
3. F. Xu, X. Ma, Q. Zhang, *et al.*, "Secure quantum key distribution with realistic devices," Rev. Mod. Phys. **92**(2), 025002 (2020).
4. P. Kok, W. J. Munro, K. Nemoto, *et al.*, "Linear optical quantum computing with photonic qubits," Rev. Mod. Phys. **79**(1), 135–174 (2007).
5. O. Alibart, V. D'Auria, M. De Micheli, *et al.*, "Quantum photonics at telecom wavelengths based on lithium niobate waveguides," J. Opt. **18**(10), 104001 (2016).
6. W. Bogaerts, D. Perez, J. Capmany, *et al.*, "Programmable photonic circuits," Nature **586**(7828), 207–216 (2020).
7. D. Pérez, I. Gasulla, P. D. Mahapatra, *et al.*, "Principles, fundamentals, and applications of programmable integrated photonics," Adv. Opt. Photonics **12**(3), 709 (2020).
8. K. H. Luo, S. Brauner, C. Eigner, *et al.*, "Nonlinear integrated quantum electro-optic circuits," Sci. Adv. **5**(1), eaat1451 (2019).
9. J. Wang, S. Paesani, Y. Ding, *et al.*, "Multidimensional quantum entanglement with large-scale integrated optics," Science **360**(6386), 285–291 (2018).
10. M. D. Eisaman, J. Fan, A. Migdall, *et al.*, "Invited review article: single-photon sources and detectors," Rev. Sci. Instrum. **82**(7), 071101 (2011).
11. L. Arizmendi, "Photonic applications of lithium niobate crystals," phys. stat. sol. (a) **201**(2), 253–283 (2004).
12. Y. Qi and Y. Li, "Integrated lithium niobate photonics," Nanophotonics **9**(6), 1287–1320 (2020).
13. P. R. Sharapova, K. H. Luo, H. Herrmann, *et al.*, "Toolbox for the design of $LiNbO_3$-based passive and active integrated quantum circuits," New J. Phys. **19**(12), 123009 (2017).
14. H. Jin, F. M. Liu, P. Xu, *et al.*, "On-chip generation and manipulation of entangled photons based on reconfigurable lithium-niobate waveguide circuits," Phys. Rev. Lett. **113**(10), 103601 (2014).
15. R. C. Alferness, R. V. Schmidt, and E. H. Turner, "Characteristics of Ti-diffused lithium niobate optical directional couplers," Appl. Opt. **18**(23), 4012–4016 (1979).
16. H. P. Chung, K. H. Huang, S. L. Yang, *et al.*, "Adiabatic light transfer in titanium diffused lithium niobate waveguides," Opt. Express **23**(24), 30641–30650 (2015).
17. S. Y. Yang, H. P. Chung, S. L. Yang, *et al.*, "Switching behavior engineerable, electro-optic directional couplers in aperiodic optical superlattice waveguides," Opt. Commun. **458**(11), 124800 (2020).
18. T. Suhara, "Generation of quantum-entangled twin photons by waveguide nonlinear-optic devices," Laser Photonics Rev. **3**(4), 370–393 (2009).
19. L. Xi, X. Zhang, F. Tian, *et al.*, "Optimizing the operation of $LiNbO_3$-based multistage polarization controllers through an adaptive algorithm," IEEE Photonics J. **2**(2), 195–202 (2010).
20. Y. Luo, R. Ge, H. Luo, *et al.*, "Polarization splitter-rotator based on multimode waveguide grating," Crystals **11**(10), 1170 (2021).
21. C. Y. Huang, C. H. Lin, Y. H. Chen, *et al.*, "Electro-optic Ti:PPLN waveguide as efficient optical wavelength filter and polarization mode converter," Opt. Express **15**(5), 2548 (2007).
22. T. J. Wang, L. M. Deng, H. P Chung, *et al.*, "Electro-optically spectrum switchable, multi-wavelength optical parametric oscillators based on aperiodically poled lithium niobate," Opt. Lett. **45**(20), 5848–5851 (2020).
23. H. P. Chung, W. K. Chang, C. H. Tseng, *et al.*, "Electro-optically spectrum tailorable intracavity optical parametric oscillator," Opt. Lett. **40**(22), 5132–5135 (2015).
24. H. P. Chung, K. H. Huang, K. Wang, *et al.*, "Asymmetric adiabatic couplers for fully-integrated broadband quantum-polarization state preparation," Sci. Rep. **7**(1), 16841 (2017).

Optics EXPRESS

25. J. H. Holland, "Genetic algorithms," Sci. Am. **267**(1), 66–72 (1992).
26. G. Fujii, N. Namekata, M. Motoya, *et al.*, "Bright narrowband source of photon pairs at optical telecommunication wavelengths using a type-II periodically poled lithium niobate waveguide," Opt. Express **15**(20), 12769–12776 (2007).
27. E. A. Ortega, J. Fuenzalida, M. Selimovic, *et al.*, "Spatial and spectral characterization of photon pairs at telecommunication wavelengths from type-0 spontaneous parametric downconversion," J. Opt. Soc. Am. B **40**(1), 165–171 (2023).
28. B. Y. Gu, B. Z. Dong, Y. Zhang, *et al.*, "Enhanced harmonic generation in aperiodic optical superlattices," Appl. Phys. Lett. **75**(15), 2175–2177 (1999).
29. Q. H. Tseng, A. Niko, T. D. Pham, *et al.*, "Broadband tunable electro-optic switch/power divider as potential building blocks in integrated lithium niobate photonics," Opt. Express **30**(11), 19121–19133 (2022).
30. M. Mitchell, *An Introduction to Genetic Algorithms* (MIT Press, MA, 1996).
31. Y. Q. Lu, Z. L. Wan, Q. Wang, *et al.*, "Electro-optic effect of periodically poled optical superlattice $LiNbO_3$ and its applications," Appl. Phys. Lett. **77**(23), 3719–3721 (2000).
32. A. S. Reddy, P. K. Agarwal, and S. Chand, "Adaptive multipopulation genetic algorithm based self designed fuzzy logic controller for active magnetic bearing application," Int. J. Dynam. Control **6**(3), 1392–1408 (2018).
33. M. Liu, R. Gao, J. Zhao, *et al.*, "A multi-population state optimization algorithm for rail crack fault diagnosis," Meas. Sci. Technol. **33**(5), 055014 (2022).
34. W. K. Burns, P. H. Klein, E. J. West, *et al.*, "Ti diffusion in Ti : $LiNbO_3$ planar and channel optical waveguides," J. Appl. Phys. **50**(10), 6175–6182 (1979).
35. G. Schreiber, H. Suche, Y. L. Lee, *et al.*, "Efficient cascaded difference frequency conversion in periodically poled Ti:$LiNbO_3$ waveguides using pulsed and cw pumping," Appl. Phys. B **73**(5-6), 501–504 (2001).
36. K. W. Chang, A. C. Chiang, T. C. Lin, *et al.*, "Simultaneous Wavelength Conversion and Amplitude Modulation in a Monolithic Periodically-poled Lithium Niobate," Opt. Commun. **203**(1-2), 163–168 (2002).
37. D. Marcuse, "Optimal electrode design for integrated optics modulators," IEEE J. Quantum Electron. QE **18**(3), 393–398 (1982).
38. M. Zhang, C. Wang, P. Kharel, *et al.*, "Integrated lithium niobate electro-optic modulators: when performance meets scalability," Optica **8**(5), 652–667 (2021).
39. M. Fiorentino, S. M. Spillane, R. G. Beausoleil, *et al.*, "Spontaneous parametric down-conversion in periodically poled KTP waveguides and bulk crystals," Opt. Express **15**(12), 7479–7488 (2007).
40. G. T. Xue, Y. F. Niu, X. Liu, *et al.*, "Ultrabright Multiplexed Energy-Time-Entangled Photon Generation from Lithium Niobate on Insulator Chip," Phys. Rev. Appl. **15**(6), 064059 (2021).
41. M. Younesi, R. Geiss, S. Rajaee, *et al.*, "Periodic poling with a micrometer-range period in thin-film lithium niobate on insulator," J. Opt. Soc. Am. B **38**(3), 685–691 (2021).
42. D. Zhu, L. Shao, M. Yu, *et al.*, "Integrated photonics on thin-film lithium niobate," Adv. Opt. Photonics **13**(2), 242–352 (2021).
43. Y. X. Lin, M. Younesi, H. P. Chung, *et al.*, "Ultra-compact, broadband adiabatic passage optical couplers in thin-film lithium niobate on insulator waveguides," Opt. Express **29**(17), 27362–27372 (2021).
44. N. Fabre, A. Keller, and P. Milman, "Time and frequency as quantum continuous variables," Phys. Rev. A **105**(5), 052429 (2022).
45. J. H. Shapiro and S. Lloyd, "Quantum illumination versus coherent-state target detection," New J. Phys. **11**(6), 063045 (2009).
46. S. Lloyd, "Enhanced sensitivity of photodetection via quantum illumination," Science **321**(5895), 1463–1465 (2008).
47. Y. C. Wei, B. H. Wu, Y. F. Hsiao, *et al.*, "Broadband coherent optical memory based on electromagnetically induced transparency," Phys. Rev. A **102**(6), 063720 (2020).
48. J. F. Dynes, W. W-S. Tam, A. Plews, *et al.*, "Ultra-high bandwidth quantum secured data transmission," Sci. Rep. **6**(1), 35149 (2016).
49. R. Sax, A. Boaron, G. Boso, *et al.*, "High-speed integrated QKD system," Photonics Res. **11**(6), 1007–1014 (2023).